Acta Cryst E CRYSTALLOGRAPHIC COMMUNICATIONS

ISSN 2056-9890

Synthesis and structure of pyridinium trichlorido(pyridine-κN)zincate(II)

Guzal Rakhmatova,[a]* Iskandar Allaberdiyev,[b] Kyzlarkhan Siddikova,[a] Jasur Makhmayorov,[c] Laylo Parmonova[c] and Anvar Xudoyqulov[c]

[a]Karshi State Technical University, 225 Mustaqillik Avenue, Karshi City, Kashkadarya region, Uzbekistan, [b]UzGTL, Guzar district, Kashkadarya region, Uzbekistan, and [c]University of Economics and Pedagogy, 13 I. Karimov Avenue, Karshi, 180100, Uzbekistan. *Correspondence e-mail: sardor.08122003@gmail.com

Received 22 June 2026
Accepted 8 July 2026

Edited by W. T. A. Harrison, University of Aberdeen, United Kingdom

Keywords: crystal structure; zinc(II) complex; pyridine; chloridozincate; Hirshfeld surface analysis; π–π stacking interactions.

CCDC reference: 2571358

Supporting information: this article has supporting information at journals.iucr.org/e

In the title salt, $(C_5H_6N)[ZnCl_3(C_5H_5N)]$, the Zn^{2+} atom is four-coordinated by one pyridine N atom and three chloride ligands, forming a slightly distorted tetrahedral $ZnNCl_3$ environment. In the crystal, the cation and anion are linked by bifurcated N—H···(Cl,Cl) and C—H···Cl hydrogen bonds, generating a supramolecular assembly that is further consolidated by π–π stacking interactions between aromatic rings. Hirshfeld surface analysis shows that H···Cl/Cl···H contacts are the dominant contribution to the crystal packing, accounting for 44.1% of the total surface contacts, followed by H···H (29.9%) and H···C/C···H (15.0%) interactions.

1. Chemical context

A large number of compounds based on transition-metal complexes with pyridine and its derivatives have been reported in the literature (Khan, 2021; Elsayed *et al.*, 2024; Zou *et al.*, 2021). Pyridine is one of the simplest heterocyclic compounds, structurally resembling benzene, in which a methine group is replaced by an N atom. It is precisely this electronegative N atom that fundamentally distinguishes pyridine from benzene, endowing it with distinct chemical properties. The pyridine scaffold is one of the most important structural elements found in numerous approved pharmaceutical drugs on the market (Khan, 2021; Temple *et al.*, 1992; El-Naggar *et al.*, 2021).

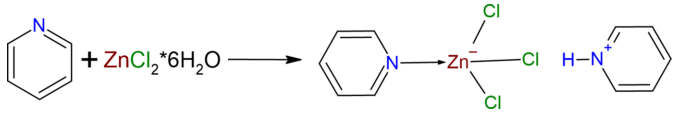

Unlike many other transition metals, the Zn^{2+} ion has a $3d^{10}$ electronic configuration, displays no redox activity and is generally far less toxic to humans, which makes it a promising basis for the development of metal-containing drugs (Porchia *et al.*, 2020). Zinc typically forms complexes with coordination numbers of 4 or 6, with tetrahedral coordination being the most characteristic geometry for this ion (Kokunov *et al.*, 2009).

In recent years, interest in the synthesis of zinc-based complexes has grown considerably owing to their favourable biological properties, with pyridine and its derivatives being among the most effective ligands for this purpose. Such complexes have been synthesized and characterized in several studies (Modec, 2018; Sun *et al.*, 2022). It has also been shown that some pyridine-based complexes exhibit higher biological activity than the corresponding free ligand. This is attributed

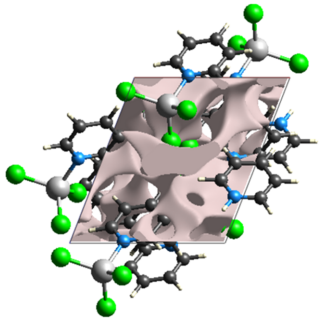

Table 1
Selected geometric parameters (Å, °).

*Cg*1 denotes the C1–C5/N1 ring and *Cg*2 denotes the C6–C10/N2 ring

Zn1—Cl1	2.2551 (7)	Zn1—Cl3	2.2451 (9)
Zn1—Cl2	2.2295 (8)	Zn1—N1	2.049 (2)
*Cg*1···*Cg*2^{i}	4.051 (2)	*Cg*2···*Cg*2^{ii}	3.824 (2)
Cl2—Zn1—Cl1	112.16 (3)	N1—Zn1—Cl1	107.33 (6)
Cl3—Zn1—Cl1	109.25 (3)	N1—Zn1—Cl2	106.42 (7)
Cl3—Zn1—Cl2	114.48 (4)	N1—Zn1—Cl3	106.76 (7)

Symmetry codes: (i) $-x+1, -y+1, -z+1$; (ii) $-x+1, -y+1, -z+2$.

to a synergistic effect between the metal centre and the biologically active ligand, as well as to an increase in the lipophilicity of the complex and, consequently, its ability to cross cell membranes. Xun-Zhong *et al.* (2020) synthesized zinc complexes with two pyridine-derived ligands that displayed higher antitumour and antibacterial activity than the free ligand. Likewise, a zinc complex based on an imino-pyridine ligand was found to exhibit higher antibacterial activity against planktonic cells of *Staphylococcus aureus* (Gram-positive) and *Escherichia coli* (Gram-negative) strains than the corresponding copper complex (de la Mata Moratilla *et al.*, 2024).

As part of our studies in this area, we now describe the synthesis and structure of the title salt, $(C_5H_6N)[ZnCl_3(C_5H_5N)]$, (**I**).

2. Structural commentary

Compound (**I**) crystallizes in the monoclinic space group $P2_1/n$ and the asymmetric unit contains one $[C_5H_6N]^+$ pyridinium cation and one $[ZnCl_3(C_5H_5N)]^-$ anion. The Zn^{2+} ion is coordinated by three chloride ions and one pyridine N atom, forming a slightly distorted tetrahedral coordination environment (Fig. 1). The Zn—N bond length is 2.049 (2) Å, whereas the Zn—Cl distances lie in the typical range observed for tetrahedral chloridozinc(II) complexes (Cotton *et al.*, 1985; Albrecht *et al.*, 2003), namely, 2.2295 (8)–2.2551 (9) Å (Table 1). The bond angles around the metal centre vary from 106.42 (7) to 114.48 (4)°, deviating from the ideal tetrahedral value of 109.47°. The largest angle is Cl2—Zn—Cl3 = 114.48 (4)°, whereas the smallest is Cl2—Zn—N1 = 106.42 (7)°. The extent of distortion is small, as confirmed by the τ_4 parameter (Addison *et al.*, 1984) of 0.946, which is close to unity for an ideal tetrahedron. As expected, the pyridine ring of the coordinated ligand is essentially planar, with an r.m.s. deviation of 0.006 Å. In the counter-ion, protonation of the N atom gives rise to a pyridinium cation, which compensates the negative charge of the complex anion.

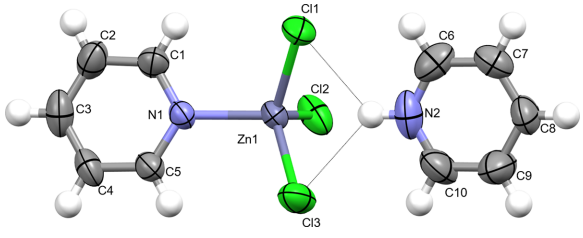

Figure 1
The molecular structure of (**I**), with displacement ellipsoids for non-H atoms drawn at the 50% probability level. Hydrogen bonds are shown as dashed lines.

Table 2
Hydrogen-bond geometry (Å, °).

D—H···*A*	*D*—H	H···*A*	*D*···*A*	*D*—H···*A*
N2—HN6···Cl1	0.86 (1)	2.74 (1)	3.389 (3)	133 (1)
N2—HN6···Cl3	0.86 (1)	2.74 (1)	3.388 (5)	134 (1)
C8—H8···Cl2^{ii}	0.93 (1)	2.92 (1)	3.681 (5)	140 (1)
C9—H9···Cl2^{iii}	0.93 (1)	2.93 (1)	3.669 (5)	137 (1)

Symmetry codes: (ii) $-x+1, -y+1, -z+2$; (iii) $-x+2, -y+1, -z+2$.

3. Supramolecular features

The crystal packing of compound (**I**) features bifurcated N—H···(Cl,Cl) hydrogen bonds, as well as non-classical C—H···Cl interactions (Fig. 2). The protonated N2 atom of the pyridinium cation acts as an efficient hydrogen-bond donor and forms a bifurcated interaction with the chloride ions of the complex anion, namely, N2—HN6···Cl1 and N2—HN6···Cl3 (Table 2). The H···Cl separations are almost the same and the Cl···H···Cl angle is 84.2 (4)°.

In addition, the packing is consolidated by two C—H···Cl contacts. Atoms H8 and H9 of the pyridine ring participate in interactions with atom Cl2 of neighbouring complex anions (Table 2 and Fig. 2). Thus, the C—H···Cl interactions complement the classical N—H···Cl contacts and generate an extended supramolecular network.

An additional stabilizing factor is provided by weak π–π stacking interactions between adjacent aromatic rings (Fig. 3), with centroid–centroid separations of *Cg*2···*Cg*2 = 3.824 (2) Å and *Cg*1···*Cg*2 = 4.051 (2) Å, where *Cg*1 denotes the C1–C5/N1 ring and *Cg*2 denotes the C6–C10/N2 ring. These values, together with the moderate interplanar angles and noticeable lateral displacement of the rings, indicate a slipped π–π stacking arrangement. Although these inter-

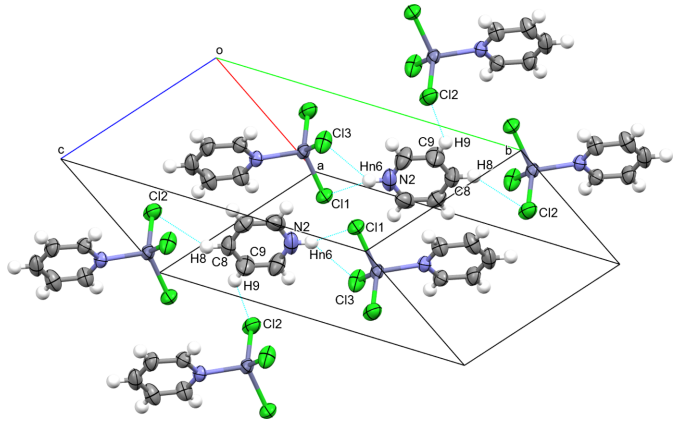

Figure 2
Supramolecular structure of (**I**), showing N—H···Cl hydrogen bonds and non-classical C—H···Cl interactions forming chains along [120].

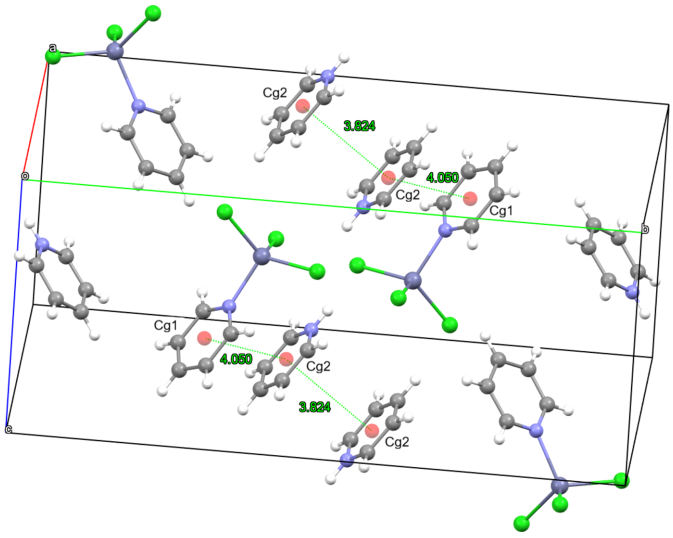

Figure 3
Aromatic π–π stacking interactions in the crystal structure of (**I**).

actions are not strong in the classical sense, they appear to make a significant contribution to the consolidation of the crystal packing.

4. Hirshfeld surface and void analysis

The Hirshfeld surface (HS) of (**I**) was calculated using *CrystalExplorer 21.5* (Spackman *et al.*, 2021). The $d_{\rm norm}$ map (Fig. 4) exhibits characteristic red spots in regions of the shortest intermolecular contacts, indicating areas where interatomic distances are shorter than the sum of the corresponding van der Waals radii. In the present structure, the most prominent contacts are associated with N—H···Cl and C—H···Cl interactions, as well as with close contacts between aromatic fragments. The blue regions on the surface correspond to intermolecular distances that exceed the van der Waals separations and therefore make a smaller contribution to the direct association of molecular fragments.

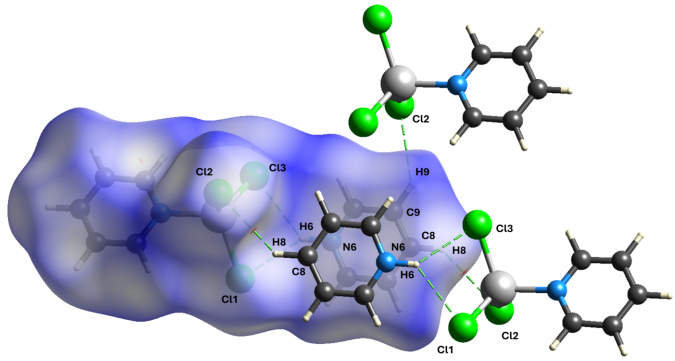

Figure 4
Hirshfeld surface of (**I**) mapped over $d_{\rm norm}$, highlighting close intermolecular contacts as red spots corresponding to regions of strong hydrogen-bonding interactions.

The total HS area and volume are 313.6 Å^2 and 338.6 Å^3, respectively. The two-dimensional fingerprint plot provides a quantitative overview of all pairwise intermolecular contacts in the crystal packing and allows the relative importance of the different interaction types to be assessed (Fig. 5). The largest contribution to the Hirshfeld surface arises from H···Cl/Cl···H contacts, accounting for 44.1% [Fig. 5(*b*)], which is fully consistent with the chloride-rich nature of the complex and the dominant role of weak hydrogen-bonding and halogen–acceptor interactions in consolidating the packing. Significant contributions are also made by H···H contacts [29.9%; Fig. 5(*c*)], reflecting van der Waals interactions between non-polar fragments, and H···C/C···H contacts [15.0%; Fig. 5(*d*)], which are generally associated with C—H···π interactions and close contacts between aromatic rings.

Smaller, but still noticeable, contributions are provided by C···C contacts (3.8%), indicating aromatic stacking; N···C/C···N (2.5%) and N···H/H···N (2.3%), reflecting the participation of N atoms in additional weak intermolecular contacts; Cl···N/N···Cl (1.0%) and Cl···C/C···Cl (0.7%), corresponding to secondary halogen-containing interactions;

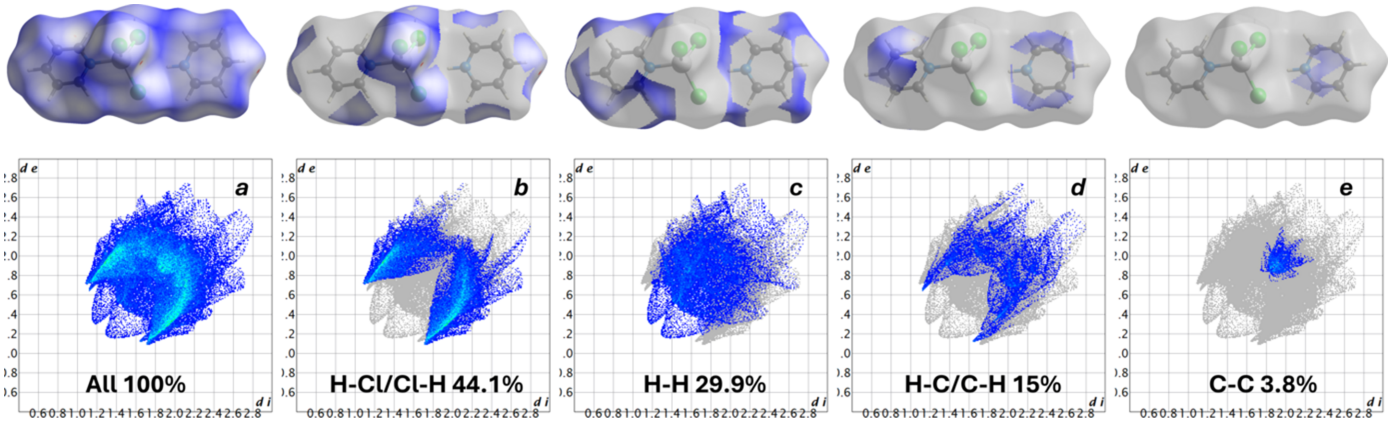

Figure 5
Two-dimensional fingerprint plots for (**I**), showing all interactions (*a*) and delineated into selected interactions: (*b*) H···Cl/Cl···H, (*c*) H···H, (*d*) H···C/C···H and (*e*) C···C, together with their relative contributions to the Hirshfeld surface.

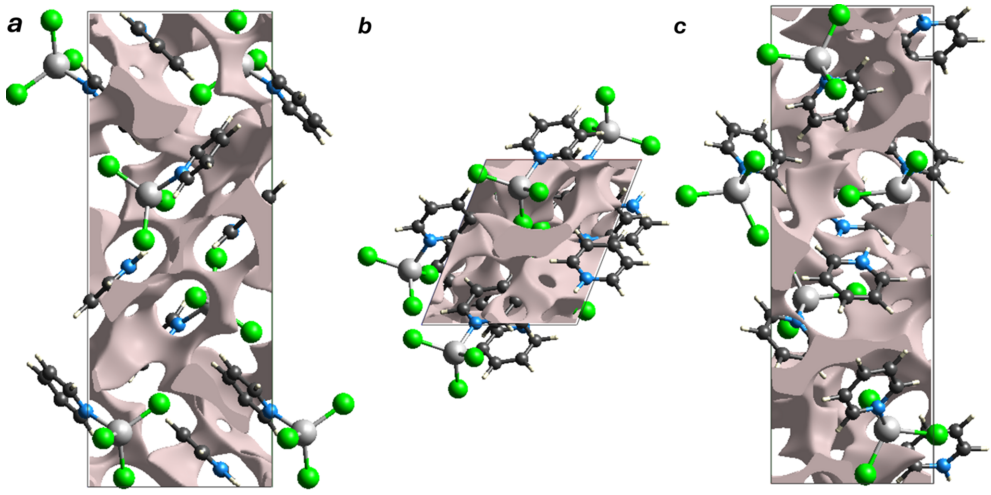

Figure 6
The void surface of (**I**).

and Zn···H/H···Zn (0.5%) and Cl···Cl (0.2%), which make only a minor contribution to the overall packing.

Void analysis based on the promolecular electron density shows that the crystal packing is relatively dense and does not contain an extended channel system (Fig. 6). The void volume is 160.5 Å^3 and its surface area is 549.6 Å^2. The identified cavities are localized and do not form a continuous porous network, indicating a predominantly compact packing arrangement in the crystal. Visual inspection of the void surface reveals that no significant voids are present between neighbouring cationic and anionic species owing to strong electrostatic attraction and the network of N—H···Cl and C—H···Cl hydrogen bonds. Instead, the void surface surrounds the ionic assembly as a whole, indicating that the residual free space is distributed around the cation–anion aggregates rather than being localized between oppositely charged fragments. The presence of such a limited void is consistent with the observed set of weak intermolecular interactions, which link the components into a stable but non-porous supramolecular motif. For density functional theory (DFT) calculations, see supporting information.

Table 3
Experimental details.

Crystal data	
Chemical formula	$(C_5H_6N)[ZnCl_3(C_5H_5N)]$
M_r	330.97
Crystal system, space group	Monoclinic, $P2_1/n$
Temperature (K)	293
a, b, c (Å)	7.80795 (16), 21.3634 (4), 8.90581 (18)
β (°)	111.418 (2)
V (Å^3)	1382.94 (5)
Z	4
Radiation type	Cu $K\alpha$
μ (mm^{-1})	7.60
Crystal size (mm)	0.62 × 0.45 × 0.20
Data collection	
Diffractometer	Rigaku XtaLAB Synergy diffractometer with a HyPix3000 detector
Absorption correction	Gaussian (*CrysAlis PRO*; Rigaku OD, 2023)
T_{min}, T_{max}	0.326, 1.000
No. of measured, independent and observed [$I \geq 2\sigma(I)$] reflections	7075, 2517, 2205
R_{int}	0.041
(sin $\theta/\lambda)_{max}$ (Å^{-1})	0.602
Refinement	
$R[F^2 > 2\sigma(F^2)]$, $wR(F^2)$, S	0.044, 0.126, 1.02
No. of reflections	2517
No. of parameters	146
H-atom treatment	H-atom parameters constrained
$\Delta\rho_{max}$, $\Delta\rho_{min}$ (e Å^{-3})	0.52, −0.73

Computer programs: *CrysAlis PRO* (Rigaku OD, 2023), *SHELXT* (Sheldrick, 2015), *olex2.refine* (Bourhis *et al.*, 2015) and *OLEX2* (Dolomanov *et al.*, 2009).

5. Database survey

A search of the Cambridge Structural Database (CSD, Version 2026.2.0; Groom *et al.*, 2016) identified five structurally related complexes. In all of these entries, pyridine or pyridine-derived ligands are present both as coordinated donors and as hydrogen-bonded species, and chloride ions are also structural components. The closest structural analogue is the zinc complex reported by Jin *et al.* (2005), in which 2-amino-5-methylpyridine acts as the ligand (CSD refcode FOBKOX). A related ruthenium complex containing the same ligand was also found (Webb *et al.*, 2013), in which two pyridine molecules are coordinated to the central metal atom together with four chloride ligands, while an additional pyridine molecule is involved in hydrogen-bonding interactions (DIPYAE).

6. Synthesis and crystallization

The following solutions were prepared: (*a*) an ethanolic solution of a $ZnCl_2{\cdot}6H_2O$ (1.0 mmol) and (*b*) an ethanolic solution of pyridine (2.0 mmol). Solution (*a*) was added to solution (*b*), and the resulting mixture was stirred at room temperature for 12 h using magnetic stirring. A crystalline precipitate was formed, filtered off, washed several times with

ethanol and dried in air. Since the obtained material was readily soluble in dimethylformamide (DMF), it was recrystallized from this solvent, yielding well-formed yellow single crystals suitable for X-ray diffraction analysis and further physicochemical investigations.

7. Refinement

Crystal data, data collection and structure refinement details are summarized in Table 3. H atoms bonded to C and N atoms were placed in calculated positions and refined using a riding model, with $U_{iso}(H) = 1.2U_{eq}(C,N)$.

Acknowledgements

We thank the Institute of Bioorganic Chemistry of the Academy of Sciences of Uzbekistan for access to the XtaLAB Synergy-S X-ray diffractometer.

References

Addison, A. W., Rao, T. N., Reedijk, J., van Rijn, J. & Verschoor, G. C. (1984). *J. Chem. Soc. Dalton Trans.* pp. 1345–1356.

Albrecht, A. S., Landee, C. P. & Turnbull, M. M. (2003). *J. Chem. Crystallogr.* **33**, 269–276.

Bourhis, L. J., Dolomanov, O. V., Gildea, R. J., Howard, J. A. K. & Puschmann, H. (2015). *Acta Cryst.* A**71**, 59–75.

Cotton, F. A., Duraj, S. A. & Roth, W. J. (1985). *Inorg. Chem.* **24**, 913–917.

de la Mata Moratilla, S., Casado Angulo, S., Gómez-Casanova, N., Copa-Patiño, J. L., Heredero-Bermejo, I., de la Mata, F. J. & García-Gallego, S. (2024). *Int. J. Mol. Sci.* **25**, 4011.

Dolomanov, O. V., Bourhis, L. J., Gildea, R. J., Howard, J. A. K. & Puschmann, H. (2009). *J. Appl. Cryst.* **42**, 339–341.

El-Naggar, M. Y., Barakat, K. M., Aly-Eldeen, M. A., Ghoneim, H. B. & Hamdan, A. M. (2021). *Egypt. J. Aquat. Biol. Fish.* **25**, 1–19.

Elsayed, M. A., Elsayed, A. M. & Sroor, F. M. (2024). *Med. Chem. Res.* **33**, 476–491.

Groom, C. R., Bruno, I. J., Lightfoot, M. P. & Ward, S. C. (2016). *Acta Cryst.* B**72**, 171–179.

Jin, Z.-M., Tu, B., He, L., Hu, M.-L. & Zou, J.-W. (2005). *Acta Cryst.* C**61**, m197–m199.

Khan, E. (2021). *ChemistrySelect* **6**, 3041–3064.

Kokunov, Y. V., Gorbunova, Y. E. & Kovalev, V. V. (2009). *Russ. J. Inorg. Chem.* **54**, 1603–1610.

Modec, B. (2018). *Crystals* **8**, 52.

Porchia, M., Pellei, M., Del Bello, F. & Santini, C. (2020). *Molecules* **25**, 5814.

Rigaku OD (2023). *CrysAlis PRO*. Rigaku Oxford Diffraction Ltd, Yarnton, Oxfordshire, England.

Sheldrick, G. M. (2015). *Acta Cryst.* A**71**, 3–8.

Spackman, P. R., Turner, M. J., McKinnon, J. J., Wolff, S. K., Grimwood, D. J., Jayatilaka, D. & Spackman, M. A. (2021). *J. Appl. Cryst.* **54**, 1006–1011.

Sun, Y. X., Zhang, W. Z., Li, J., Zhang, Y. & Dong, W. K. (2022). *Inorg. Chim. Acta* **531**, 120723.

Temple, C. Jr, Rener, G. A., Waud, W. R. & Noker, P. E. (1992). *J. Med. Chem.* **35**, 3686–3690.

Webb, M. I., Wu, B., Jang, T., Chard, R. A., Wong, E. W., Wong, M. Q., Yapp, D. T. T. & Walsby, C. J. (2013). *Chem. Eur. J.* **19**, 17031–17042.

Xun-Zhong, Z., An-Sheng, F., Fu-Ran, Z., Min-Cheng, L., Yan-Zhi, L., Meng, M. & Yu, L. (2020). *Bioinorg. Chem. Appl.* **2020**, 1–9.

Zou, X., Shi, P., Feng, A., Mei, M. & Li, Y. (2021). *Transition Met. Chem.* **46**, 263–272.

supporting information

Acta Cryst. (2026). E**82**, 919-923 [https://doi.org/10.1107/S2056989026007061]

Synthesis and structure of pyridinium trichlorido(pyridine-κ*N*)zincate(II)

Guzal Rakhmatova, Iskandar Allaberdiyev, Kyzlarkhan Siddikova, Jasur Makhmayorov, Laylo Parmonova and Anvar Xudoyqulov

Computing details

Pyridinium trichlorido(pyridine-κ*N*)zincate(II)

Crystal data

$(C_5H_6N)[ZnCl_3(C_5H_5N)]$
M_r = 330.97
Monoclinic, $P2_1/n$
a = 7.80795 (16) Å
b = 21.3634 (4) Å
c = 8.90581 (18) Å
β = 111.418 (2)°
V = 1382.94 (5) Å^3
Z = 4
$F(000)$ = 664
D_x = 1.590 Mg m^{-3}
Cu $K\alpha$ radiation, λ = 1.54184 Å
Cell parameters from 5372 reflections
θ = 4.1–67.9°
μ = 7.60 mm^{-1}
T = 293 K
Needle, metallic whiteish yellow
0.62 × 0.45 × 0.20 mm

Data collection

Rigaku XtaLAB Synergy diffractometer with a HyPix3000 detector
Radiation source: micro-focus sealed X-ray tube, PhotonJet (Cu) X-ray Source
Mirror monochromator
Detector resolution: 10.0000 pixels mm^{-1}
ω scans
Absorption correction: gaussian (CrysAlis PRO; Rigaku OD, 2023)
T_{min} = 0.326, T_{max} = 1.000
7075 measured reflections
2517 independent reflections
2205 reflections with $I \geq 2\sigma(I)$
R_{int} = 0.041
θ_{max} = 68.2°, θ_{min} = 4.1°
h = −9→9
k = −25→25
l = −10→10

Refinement

Refinement on F^2
Least-squares matrix: full
$R[F^2 > 2\sigma(F^2)]$ = 0.044
$wR(F^2)$ = 0.126
S = 1.02
2517 reflections
146 parameters
0 restraints
22 constraints
Primary atom site location: dual
H-atom parameters constrained
$w = 1/[\sigma^2(F_o^2) + (0.0897P)^2 + 0.0322P]$ where $P = (F_o^2 + 2F_c^2)/3$
$(\Delta/\sigma)_{max}$ = 0.0004
$\Delta\rho_{max}$ = 0.52 e Å^{-3}
$\Delta\rho_{min}$ = −0.73 e Å^{-3}

Fractional atomic coordinates and isotropic or equivalent isotropic displacement parameters (Å^2)

	x	*y*	*z*	U_{iso}*/U_{eq}
Zn1	0.78643 (5)	0.613782 (17)	0.66895 (4)	0.0433 (2)
Cl1	0.47863 (10)	0.60198 (4)	0.58472 (9)	0.0571 (3)

Cl2	0.89575 (11)	0.67442 (5)	0.88712 (9)	0.0681 (3)
Cl3	0.91938 (12)	0.51914 (4)	0.69616 (13)	0.0725 (3)
N1	0.8423 (3)	0.65916 (11)	0.4893 (2)	0.0421 (5)
N2	0.5590 (6)	0.46271 (15)	0.7804 (3)	0.0747 (9)
Hn6	0.5897 (6)	0.48603 (15)	0.7156 (3)	0.0896 (11)*
C5	0.9977 (4)	0.64895 (15)	0.4623 (3)	0.0506 (7)
H5	1.0755 (4)	0.61691 (15)	0.5183 (3)	0.0607 (8)*
C1	0.7294 (5)	0.70374 (14)	0.4048 (4)	0.0554 (8)
H1	0.6201 (5)	0.71076 (14)	0.4213 (4)	0.0665 (9)*
C4	1.0465 (5)	0.68401 (18)	0.3550 (4)	0.0632 (9)
H4	1.1572 (5)	0.67655 (18)	0.3411 (4)	0.0758 (10)*
C10	0.6846 (6)	0.42697 (19)	0.8822 (6)	0.0783 (11)
H10	0.8048 (6)	0.42715 (19)	0.8848 (6)	0.0939 (13)*
C7	0.3359 (5)	0.42816 (17)	0.8751 (4)	0.0644 (9)
H7	0.2158 (5)	0.42908 (17)	0.8726 (4)	0.0773 (10)*
C2	0.7691 (6)	0.73986 (17)	0.2938 (4)	0.0696 (10)
H2	0.6874 (6)	0.77067 (17)	0.2361 (4)	0.0835 (12)*
C3	0.9304 (6)	0.73001 (17)	0.2689 (4)	0.0697 (10)
H3	0.9601 (6)	0.75414 (17)	0.1949 (4)	0.0836 (12)*
C8	0.4629 (5)	0.39052 (18)	0.9809 (5)	0.0695 (10)
H8	0.4309 (5)	0.36526 (18)	1.0516 (5)	0.0834 (12)*
C6	0.3854 (6)	0.46435 (17)	0.7731 (4)	0.0726 (10)
H6	0.2995 (6)	0.49007 (17)	0.6989 (4)	0.0872 (12)*
C9	0.6370 (6)	0.3901 (2)	0.9827 (6)	0.0858 (13)
H9	0.7245 (6)	0.3640 (2)	1.0543 (6)	0.1029 (16)*

Atomic displacement parameters (Å²)

	U^{11}	U^{22}	U^{33}	U^{12}	U^{13}	U^{23}
Zn1	0.0393 (3)	0.0496 (3)	0.0467 (3)	−0.00122 (14)	0.0226 (2)	0.00252 (15)
Cl1	0.0372 (4)	0.0717 (5)	0.0634 (5)	−0.0022 (3)	0.0195 (3)	0.0042 (4)
Cl2	0.0604 (5)	0.0938 (7)	0.0588 (4)	−0.0221 (4)	0.0322 (4)	−0.0225 (4)
Cl3	0.0638 (5)	0.0561 (5)	0.1125 (7)	0.0155 (4)	0.0499 (5)	0.0212 (5)
N1	0.0444 (12)	0.0451 (13)	0.0434 (11)	0.0006 (9)	0.0238 (10)	−0.0007 (10)
N2	0.113 (3)	0.0635 (19)	0.0644 (16)	−0.0232 (17)	0.0528 (18)	−0.0023 (14)
C5	0.0450 (16)	0.0613 (19)	0.0499 (14)	0.0019 (13)	0.0226 (13)	0.0012 (13)
C1	0.0649 (19)	0.0510 (18)	0.0584 (16)	0.0149 (14)	0.0320 (15)	0.0062 (14)
C4	0.062 (2)	0.081 (2)	0.0607 (17)	−0.0117 (17)	0.0399 (16)	−0.0027 (18)
C10	0.066 (2)	0.078 (3)	0.112 (3)	−0.0001 (19)	0.057 (2)	0.005 (2)
C7	0.0515 (18)	0.066 (2)	0.081 (2)	−0.0058 (16)	0.0311 (17)	−0.0142 (18)
C2	0.099 (3)	0.057 (2)	0.0588 (18)	0.0164 (18)	0.035 (2)	0.0149 (16)
C3	0.108 (3)	0.060 (2)	0.0545 (16)	−0.019 (2)	0.0451 (19)	−0.0015 (16)
C8	0.071 (2)	0.082 (3)	0.069 (2)	−0.0076 (18)	0.0407 (19)	0.0125 (18)
C6	0.077 (3)	0.059 (2)	0.0627 (19)	−0.0010 (18)	0.0027 (18)	0.0042 (17)
C9	0.062 (2)	0.094 (3)	0.099 (3)	0.0122 (19)	0.026 (2)	0.034 (2)

Geometric parameters (Å, º)

Zn1—Cl1	2.2551 (7)	C4—C3	1.367 (5)
Zn1—Cl2	2.2295 (8)	C10—H10	0.9300
Zn1—Cl3	2.2451 (9)	C10—C9	1.343 (6)
Zn1—N1	2.049 (2)	C7—H7	0.9300
N1—C5	1.338 (3)	C7—C8	1.355 (5)
N1—C1	1.328 (4)	C7—C6	1.352 (5)
N2—Hn6	0.8600	C2—H2	0.9300
N2—C10	1.311 (5)	C2—C3	1.372 (6)
N2—C6	1.333 (6)	C3—H3	0.9300
C5—H5	0.9300	C8—H8	0.9300
C5—C4	1.373 (4)	C8—C9	1.353 (6)
C1—H1	0.9300	C6—H6	0.9300
C1—C2	1.376 (4)	C9—H9	0.9300
C4—H4	0.9300		
*Cg*1···*Cg*2^{i}	4.051 (2)	*Cg*2···*Cg*2^{ii}	3.824 (2)
Cl2—Zn1—Cl1	112.16 (3)	H10—C10—N2	120.5 (2)
Cl3—Zn1—Cl1	109.25 (3)	C9—C10—N2	118.9 (4)
Cl3—Zn1—Cl2	114.48 (4)	C9—C10—H10	120.5 (3)
N1—Zn1—Cl1	107.33 (6)	C8—C7—H7	120.3 (2)
N1—Zn1—Cl2	106.42 (7)	C6—C7—H7	120.3 (2)
N1—Zn1—Cl3	106.76 (7)	C6—C7—C8	119.4 (4)
C5—N1—Zn1	121.9 (2)	H2—C2—C1	120.3 (2)
C1—N1—Zn1	119.67 (18)	C3—C2—C1	119.4 (3)
C1—N1—C5	118.2 (2)	C3—C2—H2	120.3 (2)
C10—N2—Hn6	118.7 (2)	C2—C3—C4	118.7 (3)
C6—N2—Hn6	118.7 (2)	H3—C3—C4	120.67 (19)
C6—N2—C10	122.6 (3)	H3—C3—C2	120.7 (2)
H5—C5—N1	118.77 (17)	H8—C8—C7	120.4 (2)
C4—C5—N1	122.5 (3)	C9—C8—C7	119.3 (4)
C4—C5—H5	118.8 (2)	C9—C8—H8	120.4 (2)
H1—C1—N1	118.92 (16)	C7—C6—N2	119.2 (3)
C2—C1—N1	122.2 (3)	H6—C6—N2	120.4 (2)
C2—C1—H1	118.9 (2)	H6—C6—C7	120.4 (2)
H4—C4—C5	120.4 (2)	C8—C9—C10	120.6 (4)
C3—C4—C5	119.1 (3)	H9—C9—C10	119.7 (3)
C3—C4—H4	120.44 (19)	H9—C9—C8	119.7 (2)
Zn1—N1—C5—C4	−172.4 (2)	C5—C4—C3—C2	0.5 (4)
Zn1—N1—C1—C2	173.6 (2)	C1—N1—C5—C4	2.1 (3)
N1—C5—C4—C3	−1.8 (4)	C1—C2—C3—C4	0.5 (4)
N1—C1—C2—C3	−0.2 (4)	C10—N2—C6—C7	0.4 (4)
N2—C10—C9—C8	−1.1 (5)	C10—C9—C8—C7	0.7 (6)

N2—C6—C7—C8	−0.8 (4)	C6—N2—C10—C9	0.5 (4)
C5—N1—C1—C2	−1.1 (3)	C6—C7—C8—C9	0.2 (4)

Symmetry codes: (i) −*x*+1, −*y*+1, −*z*+1; (ii) −*x*+1, −*y*+1, −*z*+2.

Hydrogen-bond geometry (Å, º)

D—H···*A*	*D*—H	H···*A*	*D*···*A*	*D*—H···*A*
N2—HN6···Cl1	0.86 (1)	2.74 (1)	3.389 (3)	133 (1)
N2—HN6···Cl3	0.86 (1)	2.74 (1)	3.388 (5)	134 (1)
C8—H8···Cl2^{ii}	0.93 (1)	2.92 (1)	3.681 (5)	140 (1)
C9—H9···Cl2^{iii}	0.93 (1)	2.93 (1)	3.669 (5)	137 (1)

Symmetry codes: (ii) −*x*+1, −*y*+1, −*z*+2; (iii) −*x*+2, −*y*+1, −*z*+2.